View metadata, citation and similar papers at core.ac.uk

brought to you by CORE

provided by Digital Commons@Becker

Washington University School of Medicine
Digital Commons@Becker

Open Access Publications

1-1-2013

Concurrent maturation of inner hair cell synaptic Ca2+ influx and auditory nerve spontaneous activity around hearing onset in mice

Aaron B. Wong
University Medical Center Gottingen

Zhizi Jing
University Medical Center Gottingen

Mark A. Rutherford
Washington University School of Medicine in St. Louis

Thomas Frank
University Medical Center Gottingen

Nicola Strenzke
University Medical Center Gottingen

See next page for additional authors

Follow this and additional works at: http://digitalcommons.wustl.edu/open_access_pubs

Recommended Citation

Wong, Aaron B.; Jing, Zhizi; Rutherford, Mark A.; Frank, Thomas; Strenzke, Nicola; and Moser, Tobias, ,"Concurrent maturation of inner hair cell synaptic Ca2+ influx and auditory nerve spontaneous activity around hearing onset in mice." The Journal of Neuroscience.33,26. 10661-10666. (2013).
http://digitalcommons.wustl.edu/open_access_pubs/1529

This Open Access Publication is brought to you for free and open access by Digital Commons@Becker. It has been accepted for inclusion in Open Access Publications by an authorized administrator of Digital Commons@Becker. For more information, please contact engeszer@wustl.edu.

Authors
Aaron B. Wong, Zhizi Jing, Mark A. Rutherford, Thomas Frank, Nicola Strenzke, and Tobias Moser

This open access publication is available at Digital Commons@Becker: http://digitalcommons.wustl.edu/open_access_pubs/1529

Brief Communications

Concurrent Maturation of Inner Hair Cell Synaptic Ca^{2+} Influx and Auditory Nerve Spontaneous Activity around Hearing Onset in Mice

Aaron B. Wong (黃沛燊),[1,3,4] Zhizi Jing (经知孜),[1,2,3,4] Mark A. Rutherford,[1] Thomas Frank,[1] Nicola Strenzke,[1,2,3] and Tobias Moser[1,3,5,6]

[1]InnerEarLab, [2]Auditory Systems Physiology Group, Department of Otolaryngology, and [3]Collaborative Research Center 889, University Medical Center Göttingen, D-37099 Göttingen, Germany, [4]International Max Plank Research School for Neuroscience, Göttingen Graduate School for Neuroscience, Biophysics, and Molecular Biosciences, D-37077 Göttingen, Germany, and [5]Bernstein Center for Computational Neuroscience and [6]Center for Nanoscopy and Molecular Physiology of the Brain, University of Göttingen, D-37073 Göttingen, Germany

Hearing over a wide range of sound intensities is thought to require complementary coding by functionally diverse spiral ganglion neurons (SGNs), each changing activity only over a subrange. The foundations of SGN diversity are not well understood but likely include differences among their inputs: the presynaptic active zones (AZs) of inner hair cells (IHCs). Here we studied one candidate mechanism for causing SGN diversity—heterogeneity of Ca^{2+} influx among the AZs of IHCs— during postnatal development of the mouse cochlea. Ca^{2+} imaging revealed a change from regenerative to graded synaptic Ca^{2+} signaling after the onset of hearing, when *in vivo* SGN spike timing changed from patterned to Poissonian. Furthermore, we detected the concurrent emergence of stronger synaptic Ca^{2+} signals in IHCs and higher spontaneous spike rates in SGNs. The strengthening of Ca^{2+} signaling at a subset of AZs primarily reflected a gain of Ca^{2+} channels. We hypothesize that the number of Ca^{2+} channels at each IHC AZ critically determines the firing properties of its corresponding SGN and propose that AZ heterogeneity enables IHCs to decompose auditory information into functionally diverse SGNs.

Introduction

Ca^{2+} influx through $Ca_V1.3$ Ca^{2+} channels plays a pivotal role in hair cell development and function (Platzer et al., 2000; Brandt et al., 2003). Before hearing onset (approximately P12 in mice; Mikaelian et al., 1965), inner hair cells (IHCs) generate Ca^{2+} action potentials (APs) (Kros et al., 1998; Beutner and Moser, 2001; Marcotti et al., 2003). This pulsatile Ca^{2+} influx at immature synapses triggers glutamate release that drives patterned presensory activity in the developing auditory pathway (Beutner and Moser, 2001; Glowatzki and Fuchs, 2002; Johnson et al., 2005; Tritsch et al., 2007, 2010).

After hearing onset, sound stimulation generates a graded receptor potential in IHCs (Russell and Sellick, 1983; Kros et al., 1998; Oliver et al., 2006), which applies equally to the 5–20 synapses in each IHC. However, IHCs are thought to decompose the contained auditory information into functionally diverse spiral ganglion neurons (SGNs) via synapses of different properties (Winter et al., 1990; Zagaeski et al., 1994; Merchan-Perez and Liberman, 1996; Frank et al., 2009; Grant et al., 2010; Liberman et al., 2011). For example, the Ca^{2+} signals at the active zones (AZs) of a given IHC vary in amplitude and voltage dependence (Frank et al., 2009), providing candidate mechanisms for the diverse SGN response properties that enable encoding of sound over a wide range of intensities.

Here, we used fast Ca^{2+} imaging in IHCs and electrophysiology around hearing onset in mice to record changes in presynaptic Ca^{2+} signaling and postsynaptic SGN spiking. Synaptic Ca^{2+} influx became increasingly heterogeneous as a result of the emergence of AZs with greater numbers of Ca^{2+} channels around the onset of hearing, when we also found SGNs with higher spontaneous spike rates. With computational modeling of these observations and support from findings in bassoon mutants, we propose that the number of Ca^{2+} channels at the AZ is a key determinant of SGN firing properties.

Materials and Methods

Research with C57BL/6 mice as well as bassoon mouse mutants ($Bsn^{\Delta Ex4/5}$) and littermate controls (Bsn^{wt}) of either sex followed national

Received March 15, 2013; revised April 25, 2013; accepted May 11, 2013.

Author contributions: A.B.W., M.A.R., N.S., and T.M. designed research; A.B.W., Z.J., M.A.R., and T.F. performed research; A.B.W., Z.J., and T.F. analyzed data; A.B.W., M.A.R., and T.M. wrote the paper.

This work was supported by grants from the German Research Foundation through Collaborative Research Center 889 (Projects A2 to T.M. and A6 to N.S.) and the Center for Nanoscopy and Molecular Physiology of the Brain (T.M.) and by the German Federal Ministry of Education and Research through Bernstein Center Grant 01GQ1005A (T.M.). A.B.W. was supported by a Georg Christoph Lichtenberg scholarship of the state of Lower Saxony (through the "Neurosenses" program) and a scholarship from the Croucher Foundation. We thank S. Gerke, C. Senger-Freitag for expert technical assistance, and G. Hoch for developing image analysis routines. We thank Drs. A. Bulankina, T. Dresbach, and E. Neher for critical reading of a previous version of this manuscript.

The authors declare no competing financial interests.

Correspondence should be addressed to either of the following: Tobias Moser, InnerEarLab, Department of Otolaryngology and Collaborative Research Center 889, University of Göttingen Medical Center, D-37099 Göttingen, Germany, E-mail: tmoser@gwdg.de; or Nicola Strenzke, Auditory Systems Physiology Group, Department of Otolaryngology and Collaborative Research Center 889, University of Göttingen Medical Center, D-37099 Göttingen, Germany, E-mail: nstrenz@gwdg.de.

M. A. Rutherford's present address: Department of Otolaryngology, Washington University School of Medicine, St. Louis, MO 63110.

T. Frank's present address: Friedrich Miescher Institute for Biomedical Research, CH-4058 Basel, Switzerland.

DOI: 10.1523/JNEUROSCI.1215-13.2013

Copyright © 2013 the authors 0270-6474/13/331066-06$15.00/0

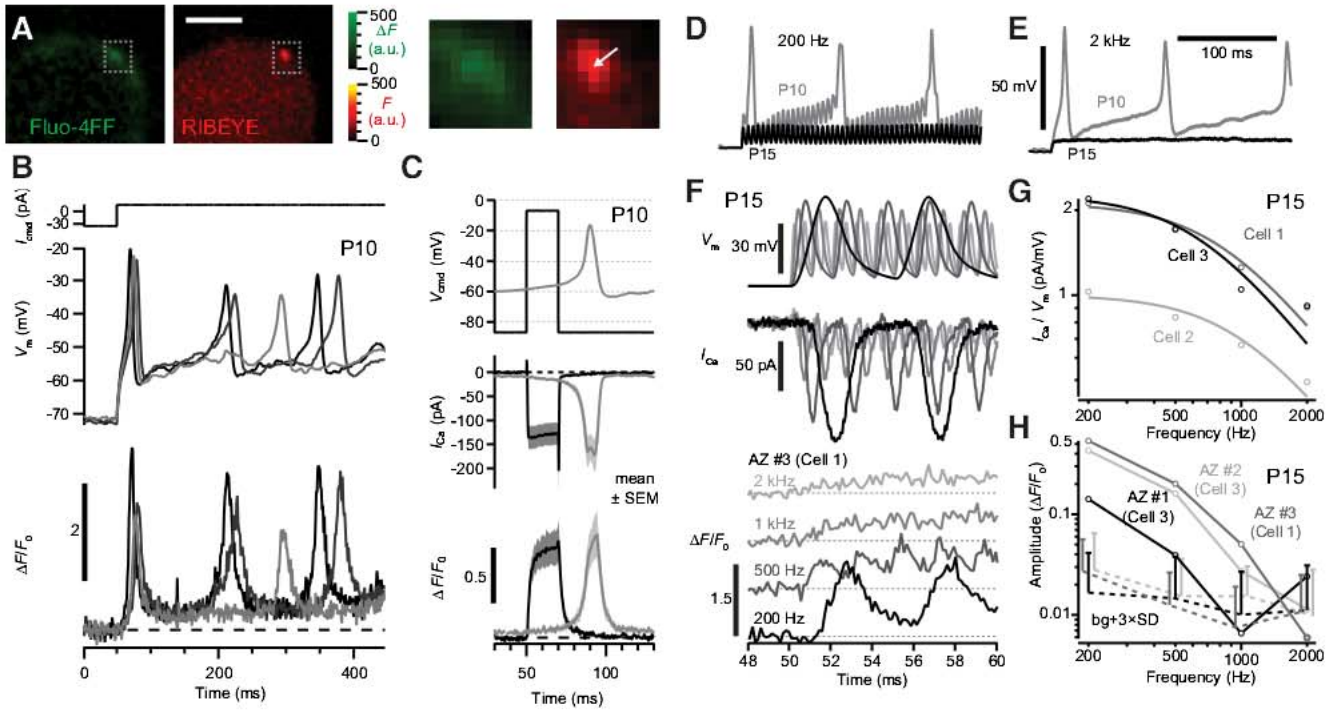

Figure 1. Naturalistic synaptic Ca^{2+} signal in IHCs before and after hearing onset. ***A***, Change in fluorescence of the Ca^{2+} indicator Fluo-4FF (green) in a P10 IHC reveals a hotspot, colocalizing with the ribbon (red) marked by the fluorescent peptide (2 μM dimer). Scale bar, 3 μm. Boxes enlarged to the right. ***B***, Small depolarizing current pulses (I_{cmd}, top) applied to a prehearing IHC elicited APs (middle), overlay of three pulses. The normalized fluorescence change of Fluo-4FF ($\Delta F/F_0$) at a synaptic ribbon indicated transient Ca^{2+} influx (bottom) during each AP. ***C***, Top, Immature IHCs were stimulated with a square depolarization or with the recorded waveform of a Ca^{2+} AP (V_{cmd}). The whole-cell Ca^{2+} current (I_{Ca}, middle) and $\Delta F/F_0$ (bottom) were similar for the two stimuli. $\Delta F/F_0$ traces are grand averages of 10 repetitions for each AZ (8 AZs in 4 IHCs). ***D***,***E***, Differential responses of the membrane potential of a P10 (gray) or P15 (black) IHC in response to inwardly rectified sinusoidal current of 200 pA peak-to-peak amplitude at 200 Hz (***D***) and 2 kHz (***E***). ***F***, The temporally compressed response of a P15 IHC to 200 Hz, 1 nA amplitude current was presented to IHCs in voltage clamp. Membrane potentials (V_m, top, corrected for attenuation as predicted by a resistor–capacitor circuit model), measured I_{Ca} (middle), and $\Delta F/F_0$ of Ca^{2+} indicator at an AZ (bottom) from a P15 IHC (AZ#3 in Cell 1, as in ***H***) stimulated at four frequencies. Robust ΔF oscillations were observable up to 500 Hz. ***G***, Amplitude of I_{Ca} (open circles) estimated as the fast Fourier transform magnitude at the stimulus frequency, normalized to V_m. Solid curves are fits to a filter function for three IHCs (see Materials and Methods). ***H***, $\Delta F/F_0$ oscillation amplitudes of three AZs from two IHCs of similar I_{Ca} amplitude, estimated as the fast Fourier transform magnitude at the stimulus frequency. Dotted lines and error bars represent the mean and variation (3× SD) of background (bg) noise within ±100 Hz of the stimulus frequency, offset on *x*-axis for clarity. In these three AZs, the $\Delta F/F_0$ oscillation fell to noise level ≤2 kHz.

animal care guidelines and was approved by the University of Göttingen Board for animal welfare and the animal welfare office of the state of Lower Saxony.

Patch clamp and confocal Ca^{2+} imaging. Patch clamp and confocal Ca^{2+} imaging of IHCs from apical coils of freshly dissected organs of Corti were performed as described previously (Frank et al., 2009). The Cs-glutamate-based pipette solution contained the following (in mM): either 10 EGTA and 0.4 Fluo-5N or 0.5 EGTA and 0.4 Fluo-4FF (Invitrogen), with 0.04 (monomer) or 0.002 (tandem dimer) carboxytetramethylrhodamine-conjugated RIBEYE-binding peptide (Francis et al., 2011). The extracellular solution contained the following (in mM): 5 or 1.3 $CaCl_2$, with 0.01 linopirdine, 0.0005 tetrodotoxin, and 0.0001 apamine for isolation of Ca^{2+} current. For current-clamp measurements, the pipette solution contained the following (in mM): 145 K-gluconate, 20 KOH–HEPES, 1 $MgCl_2$, 2 MgATP, 0.3 NaGTP, 0.5 EGTA, 0.4 Fluo-4FF, 0.002 tandem dimer peptide. The external solution contained the following (in mM): 144 NaCl, 5.8 KCl, 1.3 $CaCl_2$, 1 $MgCl_2$, 10 NaOH–HEPES, and 10 D-glucose.

Confocal Ca^{2+} imaging used *x*–*y* scans (10 Hz), spot detection (2–7.5 kHz), and line scans (0.7 kHz) (Frank et al., 2009). Quantification of line-scan $\Delta F_{Fluo\text{-}5N}$ was the average evoked change in intensity for three peak-centered pixels over the last 10 ms of depolarization. Gain of the IHC membrane input–output function for current was estimated at different frequencies with low-pass filter functions: $S = A/(1 + f^2/f_0^2)^{1/2}$, where S is signal analyzed, A is gain, and f and f_0 are stimulus and cutoff frequencies.

Immunohistochemistry. Immunohistochemistry and confocal imaging (SP5; Leica) of apical cochlear turns were performed as described previously (Frank et al., 2010) with mouse anti-C-terminal binding protein 2 (CtBP2/RIBEYE; 1:200; BD Biosciences), rabbit anti-$Ca_V1.3$ (1:75; Alomone Labs), and secondary Alexa Fluor-labeled antibodies (1:200; Invitrogen). $Ca_V1.3$ puncta intensity was analyzed as described previously (Frank et al., 2010).

Single-unit recordings from auditory nerve and cochlear nucleus. Single-unit recordings from auditory nerve and cochlear nucleus *in vivo* were performed as described previously (Taberner and Liberman, 2005; Jing et al., 2013) but adapted to younger P10–P21 mice. Under urethane/xylazine anesthesia, a glass microelectrode was advanced toward the internal auditory canal. After isolating single-unit spiking activity (using 90 dB noise bursts for P14–P21), we measured the spontaneous spike rate (during a 10–30 s silent period, depending on rate in initial 10 s) and frequency tuning by analyzing the spike rate as a function of tone frequency and intensity. SGNs were distinguished from cochlear nucleus units based on electrode position (P10–P21) and primary-like response patterns to 50 ms suprathreshold tone bursts (8 s^{-1}) at best frequency (P14–P21). The size of P10–P14 animals made it difficult to obtain a stable stereotactic position, potentially leading to the erroneous inclusion of some bushy cells with SGN-like response characteristics.

Model of hair cell synapse. For the model of hair cell synapse (adapted from Meddis et al., 1990), the release fraction k is a sigmoidal function of stimulus intensity, with 500-fold increase at saturating level based on release rate change at saturating $[Ca^{2+}]_i$ (Beutner et al., 2001). Release rate was further scaled by N_{Ca} (Ca^{2+} channel number). The spike generation probability, following an exponential distribution scaled by the cleft transmitter content c, was modulated by both absolute (0.8 ms) and relative (exponential function with $\tau = 2$ ms) refractoriness. The spike scaling parameter h was kept constant (value of 2). The model was

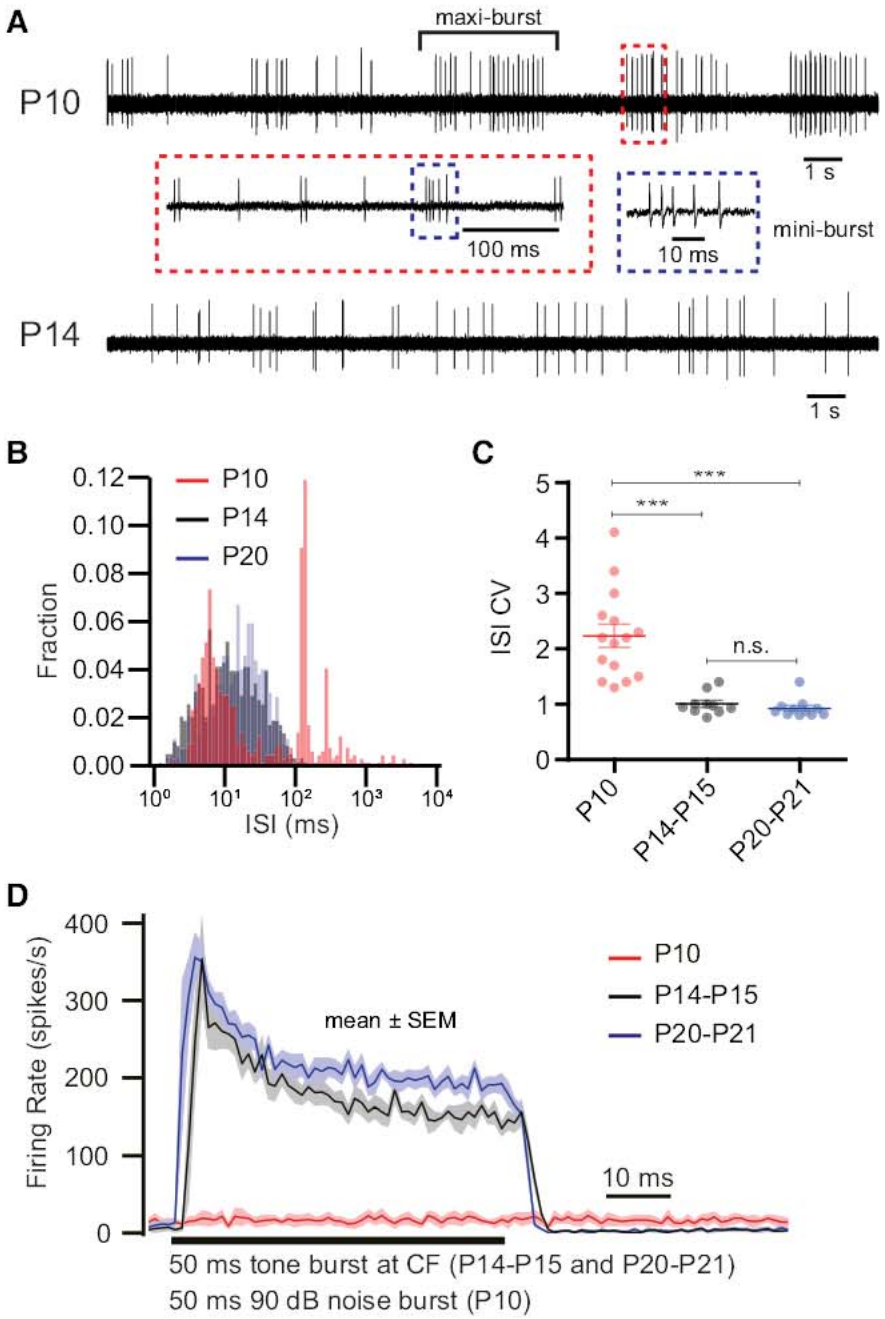

Figure 2. Developmental changes in SGN firing properties *in vivo*. ***A***, A 20 s example trace of spontaneous spiking activity of single P10 (top) and P14 (bottom) SGNs. Note the alternation between silence and active periods in P10, whereby mini-bursts cluster in maxi-bursts. ***B***, ISI histograms of representative SGNs in three age groups (red, P10; black, P14 –P15; blue, P20 –P21) during spontaneous activity. The strong peak for the P10 SGN at ~120 ms shows the inter-mini-burst interval. ***C***, CV of ISI for SGNs in three developmental age groups. A CV of ~1 is typical for a stochastic Poisson process, whereas a higher CV is related to bursting activity. n.s., No significant difference; ***$p < 0.001$. ***D***, Averaged PSTHs of SGNs in response to a 50 ms tone burst at characteristic frequency (CF; 30 dB above threshold, for P14 –P15, $n = 9$ SGNs; P20 –P21, $n = 11$ SGNs) or of a 50 ms noise burst (P10, $n = 8$ SGNs).

implemented in Igor Pro (Wavemetrics) and used to simulate post-stimulus time histograms (PSTHs) as a function of stimulus intensity for different N_{Ca}.

Data analyses. Data analyses and statistical tests were done in Igor Pro for Ca^{2+} imaging and immunohistochemistry. SGN recordings were analyzed using MATLAB (MathWorks). Normality of dataset was assessed with the Jarque–Bera test. The *F* test was used to assess equality of variance in normally distributed datasets. Unpaired, two-tailed Wilcoxon's rank test (Mann–Whitney *U* test) was used to compare non-normal or data with unequal variances. Otherwise, unpaired, two-tailed *t* tests were used. Comparison of dispersion was performed with a modified Levene's test (Brown and Forsythe, 1974). One-way ANOVA followed by Dunn's tests were used to detect differences in multiple comparisons. Data are presented as mean ± SEM, unless specified otherwise.

Results

Naturalistic Ca^{2+} signals at IHC synapses before and after hearing onset

First, we studied Ca^{2+} signals at IHC synapses labeled with a fluorescent ribbon-binding peptide (Fig. 1*A*, right). Robust Ca^{2+} transients followed the time course of changes in V_m during Ca^{2+} APs elicited in immature IHCs under current clamp (spot detection; Fig. 1*B*). The recorded Ca^{2+} APs caused a synaptic Ca^{2+} signal of amplitude comparable with that evoked by a 20 ms step command to −7 mV (Fig. 1*C*), a stimulus that elicits maximal Ca^{2+} current and triggers exocytosis of readily releasable vesicles in IHCs (Beutner and Moser, 2001).

We probed the fidelity of synaptic Ca^{2+} signals in IHCs of hearing mice with naturalistic potentials generated by inwardly rectified sinusoidal (mechanotransducer-like) currents in preceding experiments (Fig. 1*D*,*E*). We simultaneously monitored the IHC Ca^{2+} current and Fluo4-FF fluorescence using spot detection (Fig. 1*F*). Stimulus frequency was scaled by temporal compression of the response to 1 nA, 200 Hz stimulation to bypass the filtering effects of the membrane time constant. We found that the modulation of the Ca^{2+} current and the Fluo4-FF fluorescence by the receptor-potential-like stimuli declined with increasing frequency (Fig. 1*G*,*H*). Fitting a low-pass filter function to the normalized Ca^{2+} current (see Materials and Methods), we observed a cutoff frequency of 867 ± 166 Hz ($n = 3$ IHCs), which is slightly higher than that of the IHC membrane filter *in vitro* (527 ± 135 Hz, 500 pA, $V_m = -57$ mV) and *in vivo* (490 Hz; Russell and Sellick, 1983). Fluo4-FF fluorescence modulation declined at lower frequencies (Fig. 1*H*), often being visible at 500 Hz (five of eight AZs) and sometimes detectable at 1 kHz with fast Fourier transformation (Fig. 1*F*,*H*; three of eight AZs, e.g., AZ #3).

Developmental changes in the firing properties of mouse SGNs

We did not detect sound-evoked activity to noise and tone bursts up to 100 dB in P10 mice (at 10 Hz of repetition). Instead, P10 neurons spontaneously fired bursts of spikes, as shown in Figure 2*A*. As described previously for SGNs *in vitro* (Tritsch et al., 2010), spikes clustered within "mini-bursts", which were on average separated by a silent interval of ~120 ms. In addition, mini-bursts clustered into

maxi-bursts that could last for >1 s and occurred at intervals of seconds (Fig. 2A,B). Reflecting the multimodal interspike intervals (ISIs) in P10 neurons, their coefficient of variation (CV) was >1 (2.2 ± 0.2, n = 15), significantly larger than the ISI CV of Poissonian spontaneous activity in P14–P21 neurons (Fig. 2C). In comparison to P14-P15, thresholds at best frequency were lower in SGNs of P20–P21 mice ($p < 0.0001$). For both hearing age groups, best frequencies spanned ~3 octaves centered at ~12 kHz. At P20–P21 (Fig. 2D), we found shorter first spike latencies ($p = 0.01$) and a tendency toward higher peak and adapted rates ($p = 0.33$ and 0.05) compared with P14–P15 SGNs, whereas adaptation kinetics was indistinguishable ($p = 0.96$). On average, the spontaneous firing rate was lower at P10 than after hearing onset ($p = 0.02$; P10, 11.5 ± 2.1 Hz, n = 15 vs P14–P21, 24.9 ± 4.6 Hz, n = 20), whereas there was no significant difference between the older groups ($p = 0.8$; P14–P15, n = 9 vs P20–P21, n = 11). This developmental emergence of SGNs with higher spontaneous rate is consistent with findings in cats (Walsh and McGee, 1987).

Emergence of AZs with strong Ca^{21} influx

Because AZs with strong Ca^{2+} influx might "drive" the highly sound-sensitive SGNs, which also have high spontaneous rates, we tested for a developmental change in synaptic Ca^{2+} influx of IHCs. We analyzed the synaptic Ca^{2+} influx at the AZs of P10 and P14 IHCs by line scans of Fluo-5N fluorescence at fluorescently tagged ribbons during 20 ms step depolarizations to −7 mV with 10 mM EGTA in the pipette (Fig. 3A). The mean $\Delta F/F_0$ ($p = 0.007$; but not the mean ΔF, $p = 0.58$) and the dispersion of $\Delta F/F_0$ ($CV_{P10} = 0.52$, n = 58; $CV_{P14} = 0.82$, n = 75, modified Levene's test, $p = 0.0018$) were significantly greater after hearing onset (Fig. 3B). The separation between the ΔF distributions in their upper halves (Fig. 3F) indicates a selective strengthening of Ca^{2+} influx at a subset of AZs. Neither spatial spread (Fig. 3C, $p = 0.16$) nor the voltage dependence (Fig. 3D, using Fluo-4FF and spot detection, $p = 0.09$) of the synaptic Ca^{2+} signal changed significantly. For comparison, in Figure 3F, we replot the ΔF distributions acquired in IHCs of hearing-impaired mice in which the presynaptic scaffold bassoon is disrupted ($Bsn^{\Delta Ex4/5}$) and the average synaptic Ca^{2+} influx and its heterogeneity are reduced (Frank et al., 2010).

Next, we approximated the amount of $Ca_V1.3$ protein at ribbon-occupied AZs before (P6) and after (P21) hearing onset using semiquantitative immunofluorescence microscopy, identifying ribbons and juxtaposed $Ca_V1.3$ immunofluorescent spots as synapses in confocal microscopy (Fig. 3E; Frank et al., 2010).

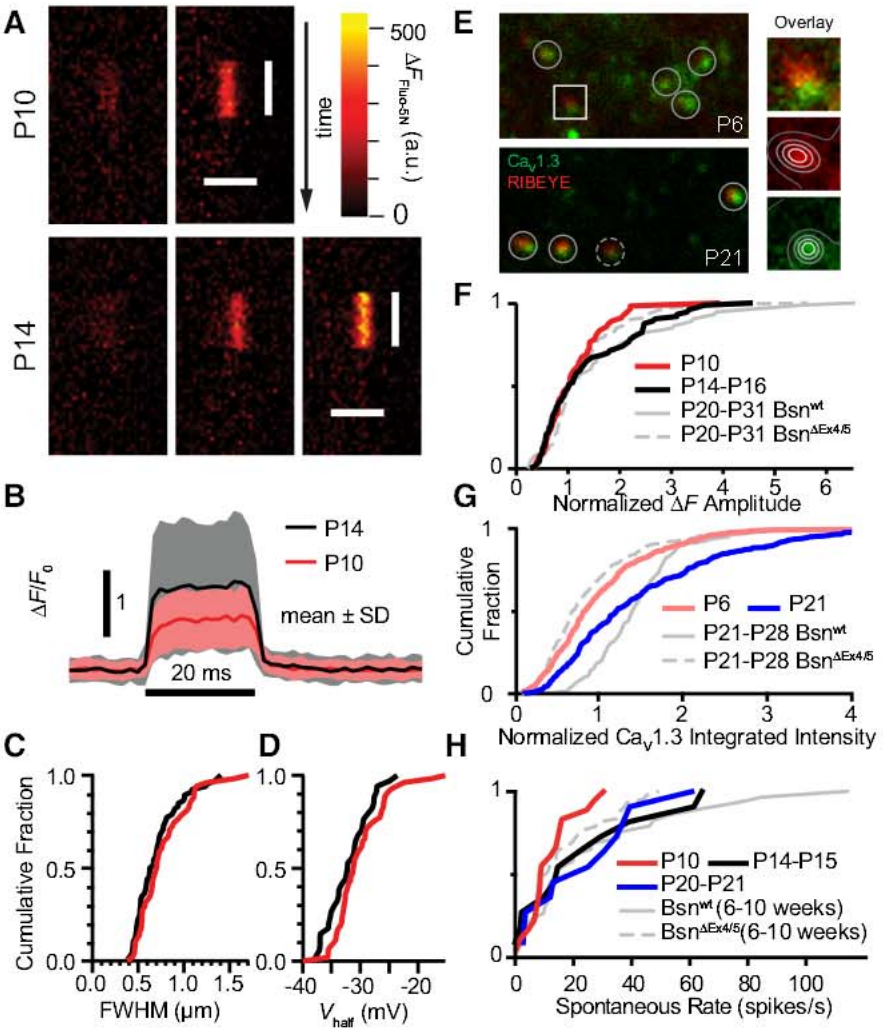

Figure 3. Developmental increase in heterogeneity of synaptic Ca^{2+} signals coincides with emergence of AZs with more Ca^{2+} channels and SGNs with higher spontaneous rates. ***A***, Examples of Fluo-5N fluorescence change ($\Delta F_{Fluo-5N}$) at synaptic sites during a 20 ms depolarization to −7 mV in prehearing (P10) and hearing (P14) IHCs, using line scans. All images were baseline subtracted (average of 50 ms period before depolarization) and have the same color lookup scale. Vertical bars indicate the duration of depolarization, and the horizontal bars indicate 2 µm. ***B***, Average temporal profile of $\Delta F/F_0$ for prehearing (P10, red trace, n = 56) or hearing (P14–P16, black trace, n = 74). Shaded bands denote mean ± SD. ***C***. Cumulative distributions of full-width at half-maximum (FWHM) of $\Delta F_{Fluo-5N}$ spatial profiles, estimated by Gaussian fit. No significant difference was found between the two age groups. ***D***, Cumulative distributions of voltage of half-activation (V_{half}) of $\Delta F_{Fluo-4FF}$ amplitude for the two age groups, estimated by Boltzmann fit. ***E***, Single confocal sections of immunolabeled tissue at P6 and P21 demonstrate an increase in Ca^{2+} channel ($Ca_V1.3$, green) accumulation around synaptic ribbons (RIBEYE, red). Right column, Two-dimensional Gaussian fit for intensity quantification (see Materials and Methods). ***F–H***, Cumulative distributions show parallel increases over postnatal development for measurements of median-normalized $\Delta F_{Fluo-5N}$ (***F***), immunofluorescence of $Ca_V1.3$ puncta (***G***), and spontaneous rate of putative SGNs of wild-type mice (***H***). Compared with mature wild-type mice, mature but hearing-impaired bassoon mutant mice ($Bsn^{\Delta Ex4/5}$) had generally smaller Ca^{2+} signals, less $Ca_V1.3$ immunofluorescence, and lower spike rates, similar to immature wild-type distributions. $Bsn^{\Delta Ex4/5}$ and Bsn^{wt} data were replotted from Frank et al. (2010) and Jing et al. (2013).

We found a developmental increase in intensity and dispersion of $Ca_V1.3$ cluster immunofluorescence, which we assume to scale with the number of $Ca_V1.3$ molecules (Fig. 3G; mean ± SD; P6, 6494 ± 3004 a.u., n = 366; P20, 7424 ± 3731 a.u., n = 359; $p = 0.004$ for mean and $p = 0.0015$ for dispersion). In conclusion, we found evidence for a gain of AZs with a large $Ca_V1.3$ channel complement accompanying the emergence of AZs with large Ca^{2+} influx around hearing onset (Fig. 3F,G).

Relating synaptic Ca^{21} signaling to firing properties of SGNs

Synaptic $\Delta F_{Fluo-5N}$ amplitudes (Fig. 3F), $Ca_V1.3$ immunofluorescence intensities (Fig. 3G), and SGN spontaneous spike

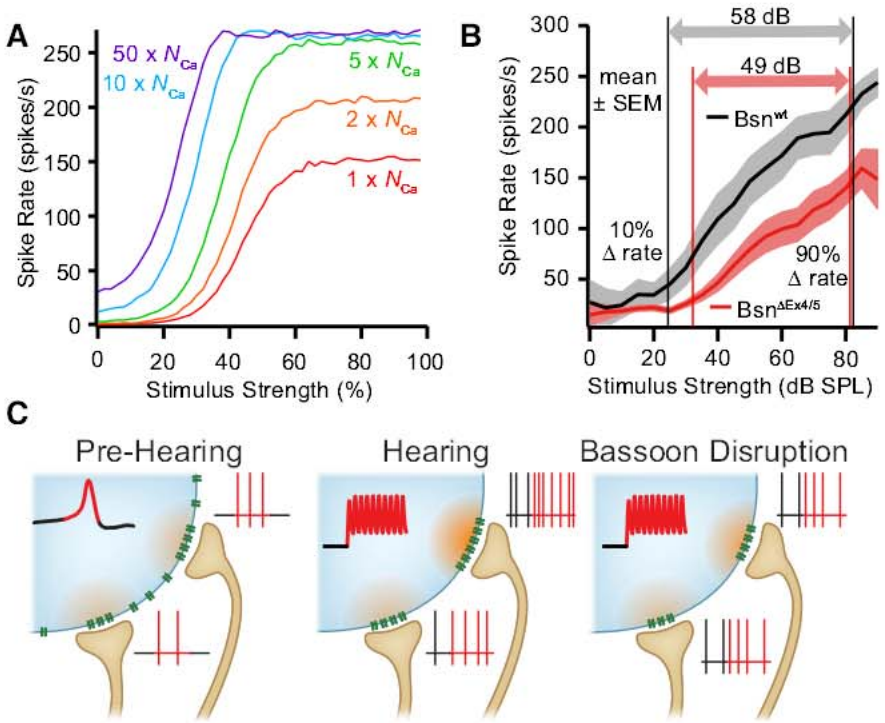

Figure 4. Ca^{2+} channel number at IHC AZs critically determines SGN firing and the combined dynamic range of SGN ensemble. ***A***, Relationship between Ca^{2+} channel number (N_{Ca}) per AZ and SGN rate-level functions in a modified model (Meddis et al., 1990) of the IHC–SGN synapse. Changing N_{Ca} can account for diversity in spontaneous spike rate, sound sensitivity, and dynamic range. ***B***, Average rate-level functions for mature wild-type and bassoon mutant mice (20 Bsn^{wt} and 20 $Bsn^{\Delta Ex4/5}$ SGNs). Arrows mark the dynamic range (10–90% between maximal and minimal rates) of the two neuron populations. ***C***, Schematic of changes in IHC Ca^{2+} signaling and SGN spiking. Concurrent with hearing onset, AZs with stronger Ca^{2+} influx emerge at wild-type synapses (middle) but not at bassoon mutant synapses (right). We propose that these strong Ca^{2+} influx sites correspond to the SGNs that have high sensitivity and spontaneous rate (purple and blue traces in ***A***).

rates (Fig. 3*H*) all increased in variability, through gain of synapses with stronger $\Delta F_{Fluo\text{-}5N}$ and immunofluorescence, and gain of SGNs with higher spontaneous rates (schematized in Fig. 4*C*). Conversely, $Bsn^{\Delta Ex4/5}$ mutants lack IHC AZs with strong Ca^{2+} signals and SGNs with high spontaneous rates (Fig. 3*F*,*H*; Jing et al., 2013).

We modified a published IHC–SGN synapse model (Meddis et al., 1990) to ask whether variations in the number of synaptic Ca^{2+} channels could account for SGN diversity. Based on the linear apparent Ca^{2+} dependence of release rate in mature IHCs (Brandt et al., 2005; Johnson et al., 2005; Keen and Hudspeth, 2006; Goutman and Glowatzki, 2007), we assumed that release scales linearly with the number of Ca^{2+} channels at the AZ in this simplified model (see Materials and Methods). The rate-level functions, calculated from the simulated PSTHs, predicted that larger Ca^{2+} channel complements alone (Fig. 4*A*, purple trace) would result in higher spontaneous spike rates and greater sound sensitivities. Interestingly, when approximating the dynamic range of sound encoding by the SGN population of $Bsn^{\Delta Ex4/5}$ and wild-type littermates across all frequencies for levels up to 90 dB SPL, we found a smaller range of encoded sound pressures in $Bsn^{\Delta Ex4/5}$ mice (49 vs 58 dB; Fig. 4*B*). The dynamic ranges and auditory thresholds of $Bsn^{\Delta Ex4/5}$ SGNs were shown previously to be normal when matched for spontaneous rate and best frequency, respectively (Buran et al., 2010; Jing et al., 2013), arguing that the reduced range of population encoding primarily reflected the lack of low-threshold, high spontaneous rate SGNs.

Discussion

Ca^{21} signals in IHCs: from presensory spiking to synaptic encoding of sound

Patterned presensory activity is a hallmark of neural development common to several sensory systems (Blankenship and Feller, 2010). In the developing auditory system, bursting activity was reported in several species (Walsh and McGee, 1987; Gummer and Mark, 1994; Lippe, 1994; Tritsch et al., 2010) and has been attributed to tightly regulated Ca^{2+} APs in immature IHCs (Kros et al., 1998; Tritsch et al., 2007; Johnson et al., 2011), which triggers IHC exocytosis (Beutner and Moser, 2001; Glowatzki and Fuchs, 2002; Johnson et al., 2005) and bursts of Na^{+} APs in SGNs (Glowatzki and Fuchs, 2002; Tritsch et al., 2007, 2010). Our Ca^{2+} imaging experiments, performed in the presence of intracellular Cs^{+} that inhibits Ca^{2+}-induced Ca^{2+} release in IHCs (Kennedy and Meech, 2002), argue for robust synaptic Ca^{2+} influx before hearing onset. Changes in Ca^{2+} indicator fluorescence at AZs of IHCs of hearing mice followed graded receptor potentials to lower frequencies than the IHC Ca^{2+} current (Fig. 1). However, our confocal Ca^{2+} imaging may underestimate the temporal fidelity of the Ca^{2+} signal driving exocytosis as a result of the limited binding kinetics of the Ca^{2+} indicator as well as spatial averaging of $[Ca^{2+}]$ within the confocal point-spread function (Frank et al., 2009).

Subcellular decomposition of auditory information in IHCs

Precisely how IHC synapses decompose auditory information toward SGNs with different sensitivities remains an important question in sensory biology (for review, see Meyer and Moser, 2010). Here we report that AZs with larger Ca^{2+} channel complement, likely enabling more intense synaptic Ca^{2+} signaling, coemerge with SGNs of higher spontaneous rate and sensitivity to sound. We also observed a developmental increase in variance for all quantities. In $Bsn^{\Delta Ex4/5}$ mice, which lack SGNs with high spontaneous rate and sound sensitivity (Fig. 3*F–H*), the IHCs have few ribbons and also lack AZs with strong Ca^{2+} signals (Frank et al., 2010). We propose that IHCs develop AZs with different ribbon sizes and Ca^{2+} channel complements, enabling differential encoding of auditory information (Fig. 4*C*). We hypothesize that AZs with many Ca^{2+} channels drive SGNs with high spontaneous rates and sensitivities. However, we do note that our study included SGNs from tonotopic regions beyond the apex, from which IHCs were recorded. In addition, other mechanisms, for example, differences in voltage dependence of synaptic Ca^{2+} influx (Frank et al., 2009), Ca^{2+} dependence or mode of release (Grant et al., 2010; Heil and Neubauer, 2010), or postsynaptic properties and regulation (Ruel et al., 2001; Liberman et al., 2011), may also contribute to SGN diversity.

References

Beutner D, Moser T (2001) The presynaptic function of mouse cochlear inner hair cells during development of hearing. J Neurosci 21:4593–4595. Medline

Beutner D, Voets T, Neher E, Moser T (2001) Calcium dependence of exocytosis and endocytosis at the cochlear inner hair cell afferent synapse. Neuron 29:681–690. CrossRef Medline

Blankenship AG, Feller MB (2010) Mechanisms underlying spontaneous patterned activity in developing neural circuits. Nat Rev Neurosci 11:18–29. CrossRef Medline

Brandt A, Striessnig J, Moser T (2003) $Ca_V1.3$ channels are essential for development and presynaptic activity of cochlear inner hair cells. J Neurosci 23:10832–10840. Medline

Brandt A, Khimich D, Moser T (2005) Few $Ca_V1.3$ channels regulate the exocytosis of a synaptic vesicle at the hair cell ribbon synapse. J Neurosci 25:11577–11585. CrossRef Medline

Brown MB, Forsythe AB (1974) Robust tests for the equality of variances. J Am Stat Assoc 69:364–367. CrossRef

Buran BN, Strenzke N, Neef A, Gundelfinger ED, Moser T, Liberman MC (2010) Onset coding is degraded in auditory nerve fibers from mutant mice lacking synaptic ribbons. J Neurosci 30:7587–7597. CrossRef Medline

Francis AA, Mehta B, Zenisek D (2011) Development of new peptide-based tools for studying synaptic ribbon function. J Neurophysiol 106:1028–1037. CrossRef Medline

Frank T, Khimich D, Neef A, Moser T (2009) Mechanisms contributing to synaptic Ca^{2+} signals and their heterogeneity in hair cells. Proc Natl Acad Sci U S A 106:4483–4488. CrossRef Medline

Frank T, Rutherford MA, Strenzke N, Neef A, Pangršič T, Khimich D, Fetjova A, Gundelfinger ED, Liberman MC, Harke B, Bryan KE, Lee A, Egner A, Riedel D, Moser T (2010) Bassoon and the synaptic ribbon organize Ca^{2+} channels and vesicles to add release sites and promote refilling. Neuron 68:724–738. CrossRef Medline

Glowatzki E, Fuchs PA (2002) Transmitter release at the hair cell ribbon synapse. Nat Neurosci 5:147–154. CrossRef Medline

Goutman JD, Glowatzki E (2007) Time course and calcium dependence of transmitter release at a single ribbon synapse. Proc Natl Acad Sci U S A 104:16341–16346. CrossRef Medline

Grant L, Yi E, Glowatzki E (2010) Two modes of release shape the postsynaptic response at the inner hair cell ribbon synapse. J Neurosci 30:4210–4220. CrossRef Medline

Gummer AW, Mark RF (1994) Patterned neural activity in brain stem auditory areas of a prehearing mammal, the tammar wallaby (*Macropus eugenii*). Neuroreport 5:685–688. CrossRef Medline

Heil P, Neubauer H (2010) Summing across different active zones can explain the quasi-linear Ca-dependencies of exocytosis by receptor cells. Front Synaptic Neurosci 2:148. CrossRef Medline

Jing Z, Rutherford MA, Takago H, Frank T, Fejtova A, Khimich D, Moser T, Strenzke N (2013) Disruption of the presynaptic cytomatrix protein bassoon degrades ribbon anchorage, multiquantal release, and sound encoding at the hair cell afferent synapse. J Neurosci 33:4456–4467. CrossRef Medline

Johnson SL, Marcotti W, Kros CJ (2005) Increase in efficiency and reduction in Ca^{2+} dependence of exocytosis during development of mouse inner hair cells. J Physiol 563:177–191. CrossRef Medline

Johnson SL, Eckrich T, Kuhn S, Zampini V, Franz C, Ranatunga KM, Roberts TP, Masetto S, Knipper M, Kros CJ, Marcotti W (2011) Position-dependent patterning of spontaneous action potentials in immature cochlear inner hair cells. Nat Neurosci 14:711–717. CrossRef Medline

Keen EC, Hudspeth AJ (2006) Transfer characteristics of the hair cell's afferent synapse. Proc Natl Acad Sci U S A 103:5537–5542. CrossRef Medline

Kennedy HJ, Meech RW (2002) Fast Ca^{2+} signals at mouse inner hair cell synapse: a role for Ca^{2+}-induced Ca^{2+} release. J Physiol 539:15–23. CrossRef Medline

Kros CJ, Ruppersberg JP, Rüsch A (1998) Expression of a potassium current in inner hair cells during development of hearing in mice. Nature 394:281–284. CrossRef Medline

Liberman LD, Wang H, Liberman MC (2011) Opposing gradients of ribbon size and AMPA receptor expression underlie sensitivity differences among cochlear-nerve/hair-cell synapses. J Neurosci 31:801–808. CrossRef Medline

Lippe WR (1994) Rhythmic spontaneous activity in the developing avian auditory system. J Neurosci 14:1486–1495. Medline

Marcotti W, Johnson SL, Holley MC, Kros CJ (2003) Developmental changes in the expression of potassium currents of embryonic, neonatal and mature mouse inner hair cells. J Physiol 548:383–400. CrossRef Medline

Meddis R, Hewitt MJ, Schackleton TM (1990) Implementation details of a computation model of the inner hair-cell auditory-nerve synapse. J Acoust Soc Am 87:1813. CrossRef

Merchan-Perez A, Liberman MC (1996) Ultrastructural differences among afferent synapses on cochlear hair cells: correlations with spontaneous discharge rate. J Comp Neurol 371:208–221. CrossRef Medline

Meyer AC, Moser T (2010) Structure and function of cochlear afferent innervation. Curr Opin Otolaryngol Head Neck Surg 18:441–446. CrossRef Medline

Mikaelian D, Alford BR, Ruben RJ (1965) Cochlear potentials and 8 nerve action potentials in normal and genetically deaf mice. Ann Otol Rhinol Laryngol 74:146–157. Medline

Oliver D, Taberner AM, Thurm H, Sausbier M, Arntz C, Ruth P, Fakler B, Liberman MC (2006) The role of BK_{Ca} channels in electrical signal encoding in the mammalian auditory periphery. J Neurosci 26:6181–6189. CrossRef Medline

Platzer J, Engel J, Schrott-Fischer A, Stephan K, Bova S, Chen H, Zheng H, Striessnig J (2000) Congenital deafness and sinoatrial node dysfunction in mice lacking class D L-type Ca^{2+} channels. Cell 102:89–97. CrossRef Medline

Ruel J, Nouvian R, Gervais d'Aldin C, Pujol R, Eybalin M, Puel JL (2001) Dopamine inhibition of auditory nerve activity in the adult mammalian cochlea. Eur J Neurosci 14:977–986. CrossRef Medline

Russell IJ, Sellick PM (1983) Low-frequency characteristics of intracellularly recorded receptor potentials in guinea-pig cochlear hair cells. J Physiol 338:179–206. Medline

Taberner AM, Liberman MC (2005) Response properties of single auditory nerve fibers in the mouse. J Neurophysiol 93:557–569. Medline

Tritsch NX, Yi E, Gale JE, Glowatzki E, Bergles DE (2007) The origin of spontaneous activity in the developing auditory system. Nature 450:50–55. CrossRef Medline

Tritsch NX, Rodríguez-Contreras A, Crins TT, Wang HC, Borst JG, Bergles DE (2010) Calcium action potentials in hair cells pattern auditory neuron activity before hearing onset. Nat Neurosci 13:1050–1052. CrossRef Medline

Walsh EJ, McGee J (1987) Postnatal development of auditory nerve and cochlear nucleus neuronal responses in kittens. Hear Res 28:97–116. CrossRef Medline

Winter IM, Robertson D, Yates GK (1990) Diversity of characteristic frequency rate-intensity functions in guinea pig auditory nerve fibres. Hear Res 45:191–202. CrossRef Medline

Zagaeski M, Cody AR, Russell IJ, Mountain DC (1994) Transfer characteristic of the inner hair cell synapse: steady-state analysis. J Acoust Soc Am 95:3430–3434. CrossRef Medline